In Situ Monitoring of the Al(110)-[EMImCl]:AlCl₃ Interface by Reflection Anisotropy Spectroscopy

Margot Guidat+,*[a] Fatemehsadat Rahide+,[b] Mario Löw,[c] Jongmin Kim,[a] Helmut Ehrenberg,[b] Sonia Dsoke,[b] and Matthias M. May[a]

Recently, Al-batteries (AlBs) have become promising candidates for post-lithium batteries, with [EMImCl]:AlCl₃ (1:1.5) as the most commonly used electrolyte. However, progress in the development of AlBs is currently hindered by the lack of understanding of its solid-electrolyte interface. Monitoring the structure of this interface under operational conditions by complementary spectroscopy could help to identify and overcome bottlenecks of the system. Reflection anisotropy spectroscopy (RAS), an optical *in situ* technique, provides access to physical and chemical properties of electrochemical interfaces on an atomistic level. Herein, we report the first example of RAS as an *in situ* characterization technique for non-aqueous battery systems, investigating an Al(110)-based model system. During chemical pre-treatment in [EMImCl]:AlCl₃, the Al(110) surface passivation film is modified. The oxide film is partially etched while an inhomogeneous passivation layer forms, increasing the surface roughness. Upon electrochemical cycling, applied potential-dependent oscillations of the anisotropy are observed and demonstrate the applicability of RAS to monitor phenomena such as plating/stripping and surface passivation in real-time.

Introduction

Al-batteries are a promising class among the post-lithium systems as they provide high specific power and energy.[1–3] Al is abundant, inexpensive, and recyclable, and it can provide a high theoretical volumetric capacity (8046 mAh cm⁻³), making it a suitable anode material.[3,4] The condition of the Al electrode substrate plays an important role in the performance of rechargeable AlBs.[4] The Al surface is initially covered by a passivation layer consisting of an amorphous, ion/electron

[a] M. Guidat,+ J. Kim, Dr. M. M. May
Institute of Physical and Theoretical Chemistry
Universität Tübingen
Auf der Morgenstelle 15
72076 Tübingen, Germany
E-mail: margot.guidat@uni-tuebingen.de

[b] F. Rahide,+ Prof. H. Ehrenberg, Dr. S. Dsoke
Institute for Applied Materials (IAM)
Karlsruhe Institute of Technology (KIT)
Hermann-von-Helmholtz-Platz 1
76344 Eggenstein-Leopoldshafen, Germany

[c] M. Löw
Institute of Theoretical Chemistry
Universität Ulm
Lise-Meitner-Str. 16
89081 Ulm, Germany

[+] These authors contributed equally.

blocking oxide (Al₂O₃).[5] Although this oxide layer suppresses dendrite formation[6] and leads to an increased electrode/electrolyte interface stability,[4] it may also hinder the aluminum plating and stripping in non-acidic and non-corrosive AlCl₃-free electrolytes, due to the low electronic and ionic conductivities of the latter.[4,7]

The [EMImCl]:AlCl₃ Ionic Liquids (IL) remain the most commonly used electrolytes in the field of AlBs. When the ratio of AlCl₃ to [EMImCl] is higher than 1, the presence of Al₂Cl₇⁻ and AlCl₄⁻ species as well as the Lewis acidity in the electrolyte medium contribute to the corrosivity of the IL. AlCl₃ also increases the electrolyte's sensitivity to humidity.[1,8] The replacement of IL electrolytes by non-corrosive electrolytes is therefore crucial and currently constitutes a bottleneck in the field of AlBs since plating and stripping of AlCl₃-free electrolytes on Al substrates encounters severe issues such as side reactions and surface passivation.[9–13] It is consequently necessary to modify the electrode/electrolyte interfaces for AlCl₃-free electrolytes to partially remove the oxide layer, allowing both the formation of the contact between electrolyte and the Al surface and the prevention of dendrite growth.

Numerous approaches for Al surface pre-treatment and designing the Al-electrolyte interface have, via *in situ* and *ex situ* characterization like *in situ* optical microscopy and X-ray photoelectron spectroscopy (XPS), already shown to improve the cycling stability and hinder dendrite formation.[14–16] The immersion pre-treatment of the Al substrate in IL has been regarded as an efficient strategy to partially remove the inactive oxide layer (Al₂O₃) covering the Al substrate and to activate the Al electrode for subsequent electrochemical cycling in IL electrolytes.[5,17,18] However, the partial removal of the Al₂O₃ layer has not proven to be sufficient to allow subsequent electrochemical cycling in AlCl₃-free electrolytes.[19] Several hypotheses could explain the origin of the absence of plating and stripping

in AlCl₃-free electrolytes comprising a non-effective pre-treatment in IL, an oxide layer reformation inside the glovebox between pre-treatment and cycling or an oxide layer reformation after immersion in non-corrosive electrolytes.[2,18] Earlier studies have already claimed that the instability and the irregular nature of the Al-IL solid-electrolyte interphase (SEI) render the pre-treatment in IL inefficient.[19]

These findings and hypotheses can, in principle, be probed by *in situ* reflection anisotropy spectroscopy (RAS). Since the latter operates at near normal-incidence reflection, its setup makes it (rather) straightforward to integrate with other techniques.[20,21] RAS, as a non-destructive optical surface analysis can, for instance, provide more insight into the evolution of the surface either during immersion pre-treatment or during electrochemical cycling inside a glovebox. In battery research, RAS has the potential to give insight into SEI formation, metal stripping/plating, as well as ion transport processes. In the working principle of RAS, linearly polarized light impinges at near-normal incidence on a single-crystalline surface.[21,22] The difference in reflectivity, Δr, with respect to two orthogonal directions in the surface plane (x, y) is then measured and scaled with the mean reflectivity, r. The surface's anisotropy can be determined according to Equation (1):

$$\text{RAS}: \frac{\Delta r}{r} = 2 \cdot \frac{r_x - r_y}{r_x + r_y} \tag{1}$$

The anisotropy of the signal can arise from both the surface and the bulk of the sample due to the penetration depth of light in the material. In the case of cubic crystals with isotropic bulk, it is possible to exclusively get information about the surface. With such a technique, changes in surface structure and surface chemistry can be studied with a time resolution of about 10 ms. Furthermore, real-time monitoring in an electrochemical environment is possible.[22] Since RAS is restricted to single crystals, the present study focuses on the evolution of Al(110) in the IL electrolyte. Previous work on the corrosion of Al foils in the presence of HCl under galvanostatic conditions has revealed that the evolution of the surface morphology and the evolution of the etching pits depends significantly on the initial morphology of the surface, its impurities and the composition of the surface oxide.[23] Performing experiments with Al single crystals allows working with surfaces that are initially highly pure with a very low surface roughness (< 0.1 nm) and a smooth and homogeneous oxide layer on top. For a more detailed understanding of RA-spectra, it is necessary to complement RAS with other surface-sensitive techniques such as XPS and scanning tunneling microscopy (STM), or computational RAS.

In this study, we first establish the experimental and computational spectra of Al(110) surfaces with different surface terminations or in different environments. In a second part, we monitor the evolution of the oxide layer upon pre-treatment in IL (1:1.5) by *in situ* RAS and we correlate the results with computational RAS, scanning electron microscopy (SEM) and energy-dispersive X-ray analysis (EDX). The third section investigates the possibility to use *in situ* RAS to study the Al(110)-IL

(1:1.5) interface during electrochemical cycling. The experimental work presented here provides the first application of RAS on a battery system.

Results and Discussion

Computational and experimental Al(110) reference spectra

A previous study has already investigated RA-spectra of clean Al(110) surfaces prepared in an ultra-high vacuum environment as well as oxygenated Al(110) surfaces.[24] It was found that the characteristic anisotropic peak at about 1.5 eV is related to bulk Al(110) (interband transition), and is weakly affected by surface oxidation. The latter reduces the strength of the peak at 1.5 eV and shifts it to 1.45 eV. After 50 Langmuir of oxygen coverage, the oxide layer becomes amorphous and optically isotropic. Hence, above this amount of coverage, no meaningful changes in the anisotropy intensities can be detected anymore. Due to the strong anisotropy arising from its bulk, studying a (110) crystalline surface by RAS is to some extent reducing its surface-sensitivity because both bulk and surface anisotropy contribute to the RA-spectrum. However, (110) remains the orientation of choice compared to the commonly used (100) and (111) surfaces, where the surface is isotropic and, therefore, does not contribute to the RA-spectrum.

To understand the sensitivity of the RA-spectra to oxygen coverage, we model Al(110) surfaces with different amounts of O atoms on top, i.e., coverage of half a monolayer (0.5 ML) and one monolayer (1 ML). Figure 1a presents the computed RA-spectra of the clean and covered Al(110) surfaces. Similar to the experimental and theoretical results of Herrmann et al., our calculation of the clean surface yields a pronounced peak at 1.48 eV.[24] However, our calculated RA-spectrum is more similar to their experimental spectrum.[24] For instance, we find a negative anisotropy at 1.2 eV, which is also shown in their experimental spectrum, but is not observed in their theoretical result.[24] In principle, we and Herrmann et al. carried out first-principles calculations within the generalized gradient approximation, and also employed the same method for the calculation of the dielectric function, i.e. the IP-RPA approach. The main difference is the number of layers of the Al(110) surface. We and they modeled 21 and 16 layers, respectively. A different study revealed that the thickness of the slab has an effect on the RAS spectrum.[25] In addition, they used a computed bulk dielectric function for the RAS calculation, while an experimental one was adopted in our calculations. Note that by increasing the oxygen coverage, the negative peak at 1.2 eV is slightly shifted to lower energies, while the intensity of the characteristic peak at 1.48 eV is proportionally reduced.

Since the oxygen concentration inside our glovebox is in the order of 0.5 ppm, the Al crystal can, due to its high reactivity, be considered to be passivated with an oxide layer. Thus, it is appropriate to compare an experimental spectrum with a theoretical spectrum corresponding to Al(110) with at least one oxygen monolayer on top.

Batteries & Supercaps

Research Article
doi.org/10.1002/batt.202300394

Chemistry
Europe
European Chemical
Societies Publishing
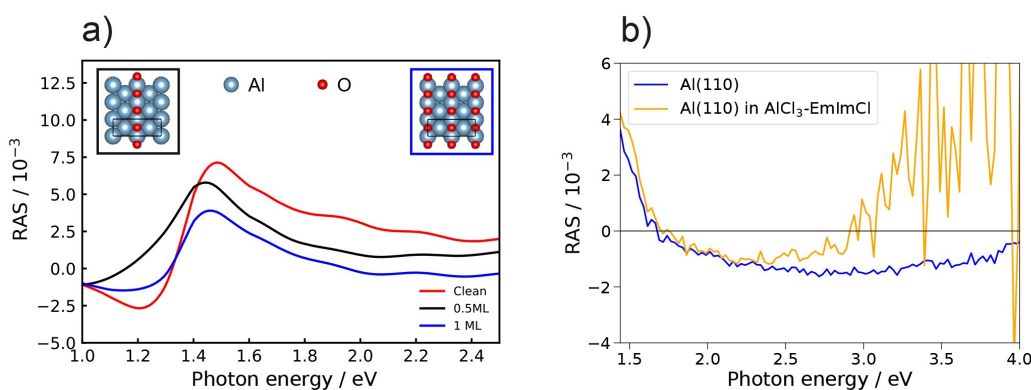
Figure 1. (a) Computed RA-spectra of the clean Al(110) (red), half monolayer (black) and monolayer (blue) coverage of O atoms on the surface. The insets show a top view of the 0.5 ML and 1 ML structures covered with oxygen. Oxygen and Aluminium atoms are depicted in red and light blue, respectively. The unit cells are indicated by the black lines. (b) Reference spectra of the Al(110) surface in Argon atmosphere and of the Al(110)-IL interface directly after immersion.

Figure 1b shows the experimental reference RA-spectra corresponding to the Al(110) surface and the Al(110)-IL interface. The reference spectrum of the as-received Al(110) crystal shows the same characteristics as the theoretical spectrum shown in Figure 1a. The anisotropy intensity is similar to the one of a monolayer oxygen coverage, suggesting that an oxide layer of about one monolayer passivates the Al surface. Since the resolution of the RA-spectra is significantly impacted by the setup, i.e. by the presence of a thick and coloured electrolyte layer, the data presented in this paper have a low signal-to-noise ratio. In particular, the spectrum of Al(110) in the IL suffers from a low signal-to-noise ratio beyond 3.0 eV due to the light absorption from the electrolyte at these energies. Moreover, due to the energy-range limitation of the spectrometer, it is not possible to access energies below 1.44 eV. Therefore, all the following graphics are restricted to an energy range between 1.44 and 2.5 eV, which allows better visibility of the area of interest. Figure 1b exhibits a small anisotropy offset already in the energy range of 1.44–3.0 eV when Al(110) is immersed in IL.

Since the bulk electrolyte is not expected to be structured and should, therefore, not contribute to the optical anisotropy in this energy range, the anisotropic offset is expected to originate from an imperfect baseline correction or from a linear electro-optic effect from structured electrolyte molecules acting as dipoles at the near-Al surface. Further explanations are the dependence of the chemical interactions between the surface and the electrolyte, resulting in a modification in the morphology or composition of the surface.

Surface pre-treatment

For the surface pre-treatment, continuous RA-spectra (colour-plot) were recorded over the time for 2 h of immersion of the Al crystal C1 in IL and are presented in Figure 2a. On the colourplot (CP), changes related to the peak at 1.5 eV are observed upon immersion. The width of the peak is conserved, but its anisotropy drops in the first phase before increasing
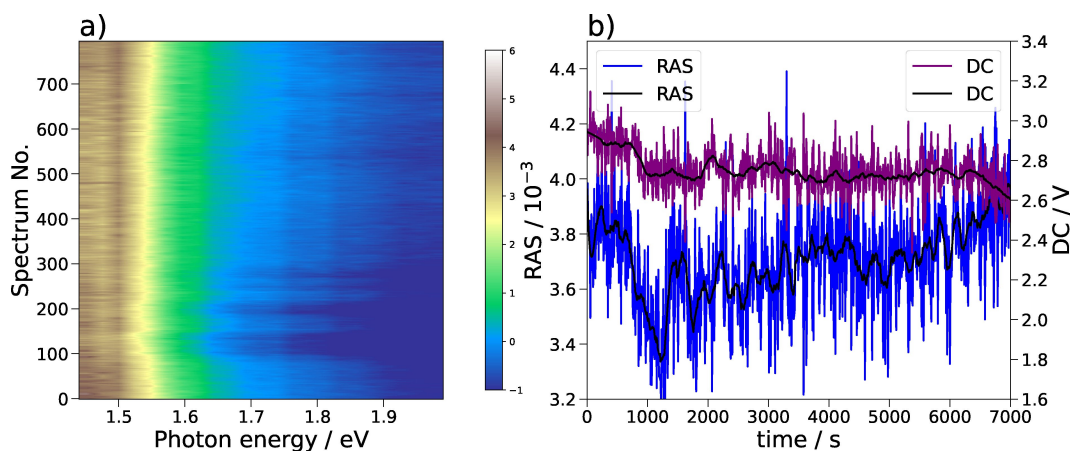
Figure 2. (a) Colourplot (CP) of Al(110) upon immersion in IL for 2 h. (b) Transient at 1.49 eV extracted from the CP. The purple and blue curves correspond to the evolution of the anisotropy and the reflectance over the time, respectively. The black curves correspond to the transients data filtered with a Savitzky–Golay filter.

slightly above its initial value. For better visibility on the trend of the CP, a transient at 1.49 eV together with the reflectance (proportional to the DC signal) over the time at 1.49 eV are extracted and shown in Figure 2b. Here, the decrease in the anisotropy and the reflectance until the first half hour of the pre-treatment is noticeable, i.e. the interface deteriorates over time. The loss in the interface ordering is expected to originate from partial oxide layer removal and electrolyte decomposition. Previous studies have shown that after immersion or cycling of Al in IL, the Al surface contains a trace amount of chlorine from residual electrolyte that adsorbs on the oxide layer.[26,27] Furthermore, due to trace amounts of water originating from the glovebox atmosphere, $AlCl_3$ undergoes a hydrolysis leading to the formation of $Al(OH)_3$, Al_2O_3, and HCl, which can affect the Al-IL interface.[26] In the second phase, the anisotropy rises until slightly above its initial value at the end of the pre-treatment, meaning that the ordering at the interface. The rupture of the oxide film that partially dissolves in the electrolyte and then leads to the appearance of active sites on the surface would explain the increase of the RA intensity at the end of the pre-treatment. Concerning the DC signal, it progressively decreases until the end of the pre-treatment, confirming that the increase in ordering at the interface does no occur homogeneously over the surface plane and that some areas of the interface keep deteriorating. The formed solid electrolyte interface consisting of the byproducts of the IL electrolyte and repassivated Al_2O_3 oxide film on the Al surface complicates the interpretation of the RA-spectra. Hence, we will in the following refer to the layers present on the Al surface as the passivation layer. To minimize the contribution of the electrolyte film to the spectra, a comparison of spectra and SEM pictures taken before and after pre-treatment (in the absence of electrolyte) is shown in Figure 3.

Figure 3a–b compares the RA-spectra and the DC signals of the Al(110) surface before and after pre-treatment in IL, as well as the relative ratio of the RA-spectrum taken after pre-treatment, divided by the one taken before pre-treatment and the difference between the DC signals. The DC signal is proportional to the reflectance of the Al surface and correlating

it with the anisotropy can help understanding the surface evolution. In Figure 1a, apparent changes in the peak at 1.5 eV between non-treated and treated surfaces are displayed. An increase of the anisotropy after pre-treatment is observed. According to the results discussed in Figure 1a, this increase indicates a reduction in oxygen coverage. A comparison of the RA-intensities between the theoretical and experimental spectra suggests that the crystal is initially covered by about one monolayer of oxygen. After pre-treatment, the anisotropy maintains a value between 4 and 5 at 1.5 eV, suggesting that the surface is still partially covered by oxygen after pre-treatment. Taking into account the oxygen content from the glovebox atmosphere, it is to be expected that surfaces re-oxidize after pre-treatment.

For a better understanding, the evolution of the anisotropy is compared to the evolution of the DC signal before and after pre-treatment (Figure 3b). An increase in reflectance and anisotropy implies, according to Figure 1a, a progressive removal of an oxide layer, leaving behind a cleaner surface. However, as depicted in Figure 3a–b, the DC signal decreases after pre-treatment while the RAS signal increases, which is a typical signature of surface roughening. Moreover, it is important to notice that both the RA-spectra ratio and DC signals difference lead to a rather constant value over the whole photon energy range. It suggests that either the surface is getting rougher, rather than its passivation layer reduced or the increase in surface in-homogeneity is more prominent in the evolution of the RA-spectrum than the reduction in the passivation layer thickness. These observations are in agreement with the conclusions from Natishan et al. on the reaction mechanism between chlorine and Al/Al_2O_3 in chlorine-containing electrolytes.[28] They demonstrated that after its adsorption on Al_2O_3, Cl^- is incorporated into the bulk of the oxide and moves towards the oxide/metal interface. Afterwards, Cl^- reaches the oxide/metal interface leading to blister formation and rupture of Al_2O_3 oxide film. The rupture of the oxide film, however, occurs only locally and leads to a heterogeneous, porous oxide layer with pitting corrosion. Assuming a similar mechanism on the oxidized Al(110) surface in the presence of
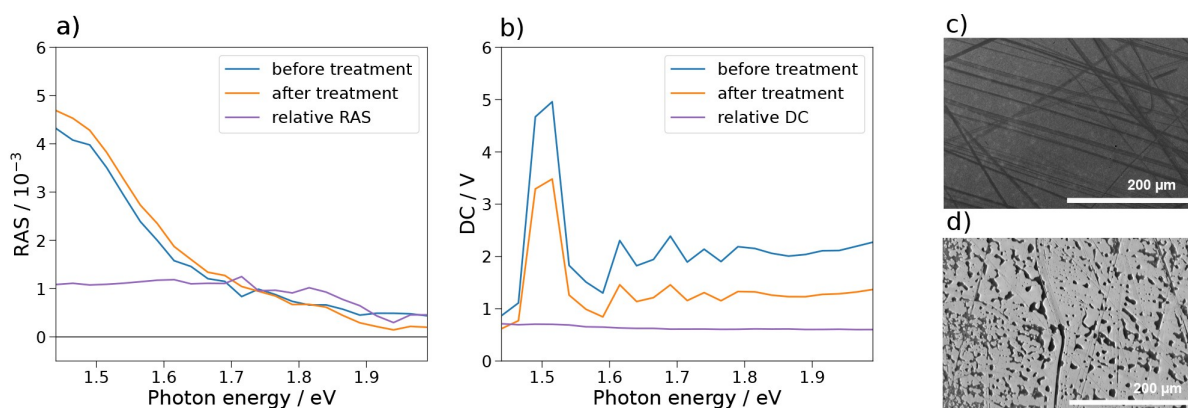
Figure 3. RA-spectra and their ratio (a) and DC signals and their absolute difference (b) of Al(110) surface before and after pre-treatment in IL. (c) and (d) provide the SEM pictures taken before and after pre-treatment, respectively.

Batteries & Supercaps

Research Article
doi.org/10.1002/batt.202300394

Chemistry
Europe
European Chemical
Societies Publishing

$Al_2Cl_7^-$ and $AlCl_4^-$ species would explain why not only the surface roughness increases, leading to an overall increase in the anisotropy, but also the anisotropy increases at around 1.5 eV due to the appearance of clean Al(110) surface spots. This interpretation implies that the surface is getting inhomogeneous on a microscopic scale.

To complement our findings from the RAS data, SEM pictures and EDX analysis were performed on the Al crystal after it was pre-treated and clean-connect transferred to the SEM chamber. Figure 3c–d compares the SEM pictures of the crystal before (as received from the supplier) and after pre-treatment, respectively. On the picture from Figure 3c, the as-received Al surface presents some scratches from the last polishing steps performed by the supplying company during the surface preparationof the crystal. The surface also contains particles of less than 1 μm in size composed of SiO_2. Since the last polishing step for Al crystals usually involves the use of a SiO_2 particle suspension, the presence of these particles is also attributed to residuals from the surface preparation process.[29] Figure 3d differs considerably from 3c in morphology and composition. The picture taken after pre-treatment shows an inhomogeneous surface made of a gray matrix with dark puddles on top. Displayed on Figures S2, S3 and Table S1, the EDX analysis of the same area indicates that grey matrix is composed almost exclusively of Al with low amounts of C, O and Cl (below 1 atomic weight %), while the dark areas present significant amounts of C (6–7 weight %), O (3–4 weight %), N (2–4 weight %) and Cl (4–5 weight %) and a decrease in Al content. It indicates that the pre-treatment of Al in the IL leads to the emergence of active site areas and areas where the electrolyte decomposes and adds on to the initial surface oxide layer. These results match our RAS interpretation as well as those of earlier studies.[9,19]

The change in anisotropy and reflectance upon surface pre-treatment indicates that RAS is sensitive to the evolution of the Al(110) surface in IL and allows *in situ* access. Yet the formed interface/interphase is very complex and the interpretation of the spectra is not straightforward. Furthermore, since our spectrometer averages over the whole measurement spot of several mm², the measurements average over in-plane surface inhomogeneities. Therefore, it is not possible to disentangle if the changes in the anisotropy over the pre-treatment are homogeneously distributed on the surface or are a sum of contributions from inhomogeneous areas on the surface. A parallel *in situ* investigation with reflection anisotropy microscopy (RAM) would provide a better spatial resolution and allow the elucidation of the different contributions. However, it would require, in addition to the spectrometer detector and the UV-visible light source, the inclusion of a camera, an objective lens, and a laser light source. Combining spectroscopy and microscopy is not achievable with our commercially available spectrometer but could, in principle, be implemented in a custom-build reflection anisotropy setup. Although they are currently limited to single-wavelength studies, RAM or 2D-surface optical reflectance (2D-SOR) have already demonstrated surfaces monitoring with spatial resolutions of about 5–10 μm.[30,31]

Electrochemical cycling

In the previous section, the pre-treatment of the Al(110) single crystals in IL monitored by RAS has shown that RAS is sensitive to the Al surface evolution. This suggests that it should be feasible to study *in situ* the Al(110)-IL interface/interphase during plating and stripping with RAS. To compare the electrochemical cycling behaviour of Al single crystals with the one of Al foil – which is commonly used in the AlBs community and shown in Figure S4 – Al(110) crystal number 2 (C2) is cycled in the photoelectrochemical (PEC) cell at a scan rate of 20 mV/s in a potential range allowing full Al stripping. In parallel with the cyclic voltammetry (CV), a CP is recorded at a speed that four spectra are obtained during one full potential cycle. The experimental procedure is illustrated in Figure S1. The CVs depicted in Figure 4 resemble the one with Al-foil taken in similar conditions (Figure S4), indicating that the behaviour of a (110)-oriented Al surface during electrochemical cycling is comparable to a polycrystalline Al surface. The evolution of the surface roughness observed in the RA-spectra over the experimental series can first be understood from the evolution of the CVs. Over the experimental series, the stripping peak on the CV around 0.28 V vs. Al gets more pronounced. This phenomenon is attributed to a progressive Al plating and stripping from a nanocrystalline to microcrystalline form of Al,[32] i.e. the surface is getting rougher. Thus, if the structure of the surface evolves upon cycling with an increasing amount of Al plated and stripped in a microcrystalline form, the plating and stripping occur in a more defined manner, and the variation of the anisotropy is supposed to be higher. However, because of the high scan rate and the large energy range chosen for this set of experiments, the time resolution is too low to observe a trend related to plating and stripping on the CPs recorded in parallel to the CVs (Figure S5).

During the experimental series, the CVs were recorded on both treated and untreated Al(110). As described in the pre-treatment section, when the Al(110) electrode is immersed in IL, the native Al_2O_3 film covering the Al single crystal undergoes a transformation, resulting in a porous film composed of an inner
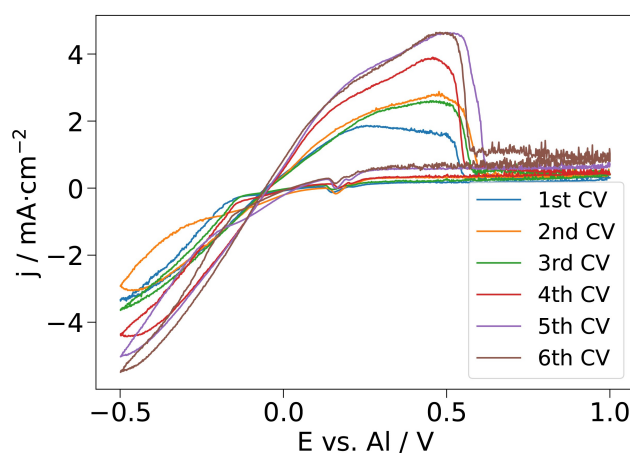
Figure 4. Last cycles of 6 CV experiments measured between −0.5 to 1 V vs. Al at 20 mV/s for 10 cycles.

Batteries & Supercaps

Research Article
doi.org/10.1002/batt.202300394

Chemistry Europe
European Chemical
Societies Publishing

layer enriched with oxides and an outer layer made of both inorganic and organic materials. According to the literature, the partial removal and the reduction in thickness of the Al_2O_3 film makes it easier for charge carriers and ions to move between the Al electrode and the electrolyte.[9,27,33,34] Figure S6 provides insights into the electrochemical behaviour of pre-treated and unpre-treated Al(110) C2 in IL under the same cycling conditions as the one of Figure 4. Specifically, it illustrates notable differences in CVs of these electrodes and their implications for the Al plating and stripping processes.

When examining the CVs of not pre-treated Al(110) in Figure S6a, it is apparent that as the cycle number increases, the current density responsible for Al plating and stripping keeps increasing. This fluctuation indicates an unstable electrode-electrolyte interface, which has a detrimental effect on the plating and stripping processes. This trend aligns with the literature, where it is stated that Al plating and stripping peaks tend to be smaller and less predictable during the initial cycles, but become more reversible with continued cycling, typically around the second or third cycle.[35,36] The native Al_2O_3 film delays the activation of the anode and makes it more challenging to reach a reversible regime, resulting in a significant over-potential.[2,37] Therefore, the result confirms that the presence of the Al_2O_3 film can act as a barrier, limiting the effective interaction between the Al electrode and the electrolyte, and reducing the efficiency of the electrochemical system.[9,36]

In Figure S6b, the maximum of the stripping peaks initially decreases over the first cycles before reaching a stable value. This is an indicator for an efficient modification or removal of the Al_2O_3 oxide layer, which is known to play a crucial role in these electrochemical processes. Hence, the porous surface film formed during the immersion pre-treatment seems to have a beneficial impact on the electrode's performance.[9]

A further set of experiments was performed on a second Al(110) crystal (C3) and was monitored with higher temporal spectroscopic resolution than for C2. In this second experimental series, Al(110) C3 is first pre-treated according to the procedure described in the experimental section. For the cycling performance, the Raman cell from rhd instruments (rhd cell) is used, where a thinner electrolyte layer is present on top of the crystal surface, reducing light absorption from the electrolyte in comparison to the PEC cell. Compared to the previous experiment series (with PEC cell), the cell is cycled at lower scan rates of 2.5 mV/s, and RAS is measured in parallel with higher temporal resolution, as depicted in Figure 5 for a potential range between −0.25 and 0.25 V vs. Al. The potential range of the CV shown in Figure 5a and 5c does not allow for complete Al stripping, but a more detailed *in situ* investigation of the surface during plating and stripping is possible from the spectroscopic side, i.e. about 20 spectra are measured per cycle, as shown in Figure 5b and 5c.

Plotting the applied voltage as a function of the time together with the CP is a systematic way to probe potential direct correlations between the electrochemical and optical measurements. In the case of systems with a high degree of ordering, such as InP in contact with low-concentration acidic electrolytes, there are clear visual correlations between the cyclic potential and the oscillations of the RA-values.[38] For Al in IL, a more complex and less ordered system, plotting the applied voltage with the CP simply helps deducing that they do exhibit a directly apparent correlation and that more extensive analysis of the CP is required. For better visibility of the anisotropy features, transients at 1.49 eV are extracted from the CPs. Figure 6 presents the electrochemical cycling of Al(110) sample C2 between −0.25 to 0.25 V vs. Al (a) and between −0.5 and 0.5 V vs. Al (b), plotted over time together with a transient and a DC-signal extracted from the CP at 1.49 eV.

To reduce the background noise from the transients shown in Figure 6, and to identify if there is a feature correlated to plating and stripping, the transients are filtered by Fast Fourier transform (FFT). The FFT-filtered transient from Figure 6a was extracted from the CP of Figure 5b at 1.49 eV and exhibits an increasing trend in the first cycles. While the anisotropy progressively decreases after the third cycle, small oscillations with a period matching the cycling period of the potential start to appear. The periods of the potential applied during the
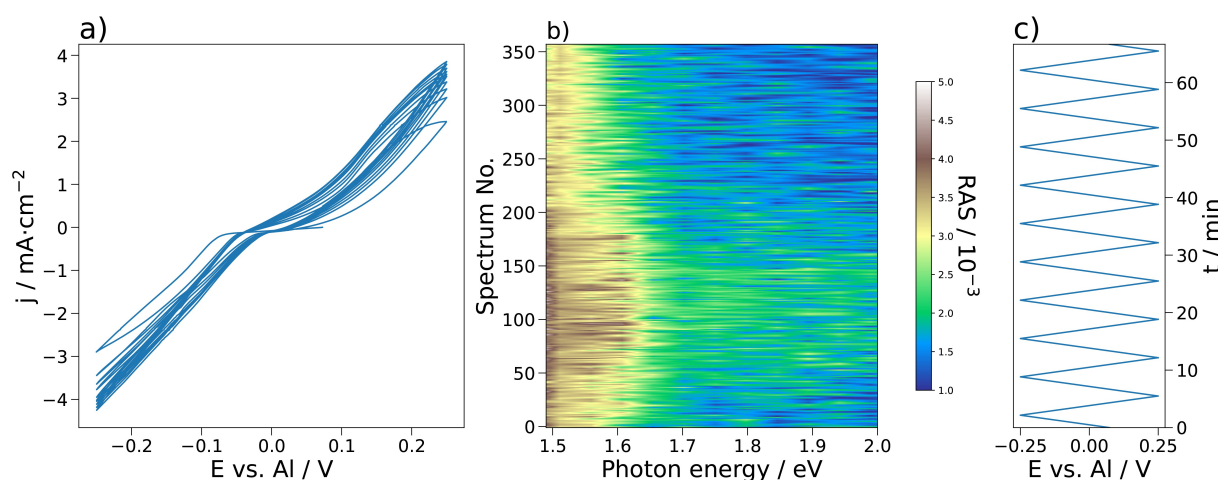
Figure 5. (a) CV between −0.25 and 0.25 V vs. Al for 10 cycles at 2.5 mV/s. (b) CP measured in parallel to CV. (c) applied voltage with respect to the time.
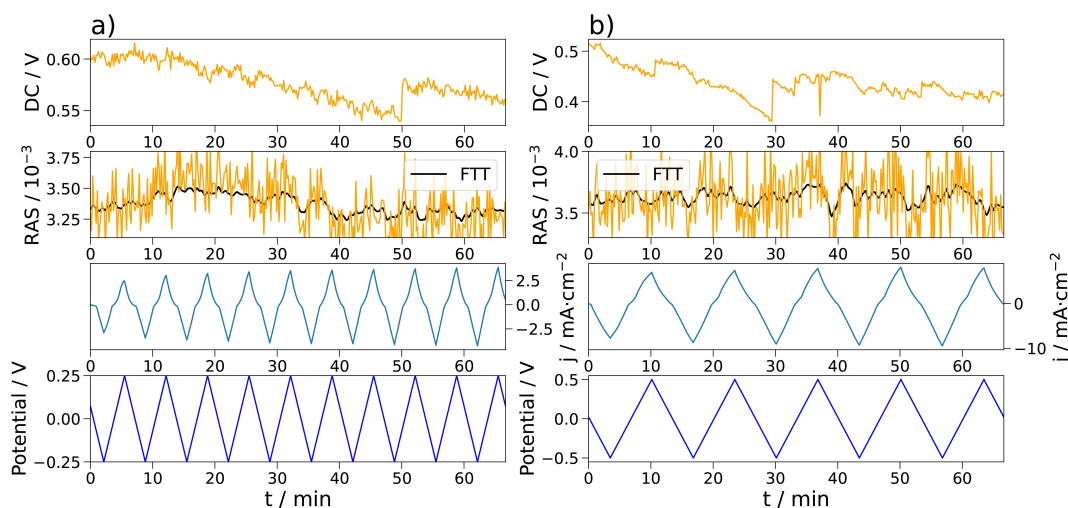
Figure 6. DC signal and transients at 1.49 eV extracted from a CP measured during (a) CV between −0.25 and 0.25 V at a scan speed of 2.5 mV/s for 10 cycles and (b) CV between −0.5 and 0.5 V at 2.5 mV/s for 5 cycles. The black curves correspond to the FFT-filtered transients.

experiments shown in Figure 6a–b are 2.5 and 1.25 mHz, respectively.

Figure 7a shows again the original transient of Figure 6a while its Fourier spectrum is shown in Figure 7b. The DC value at 0 Hz has been discredited due to its high amplitude as compared to the other peaks. The second most dominant peak is observed at 2.5 mHz, which corresponds to the oscillation period of the applied potential. The same conclusion is drawn when examining the FFT of the original transient of Figure 6b: the most prominent peak is observed at 1.25 mHz, i.e. the period of the applied potential (Figure S8).

The presence of these peaks justifies the application of an exponential filter to the data and confirms that the oscillations observed in the transient can be correlated with the applied potential. When correlating the RAS oscillations in Figure 6a with the corresponding CV, the local minima of the oscillations are located shortly after the local maxima in the anodic current. Oscillations of the RAS intensity are also present on the

transient from Figure 6b for which the potential range of the CV was broader. However, the period of the oscillations is less well-defined than for the narrower potential range. This indicates that, depending on the potential range in which Al is cycled, the plating and stripping process is more or less ordered. Between −0.25 to 0.25 V, small oscillations emerge with increasing cycle number, meaning that the process is most probably happening homogeneously at the surface and in a layer-by-layer manner.

Between −0.5 and 0.5 V, the build-up and build-down of an anisotropy are less defined, indicating that the process occurs on a larger scale and that the surface is getting rough. The DC signals globally decrease over time, but exhibit some features, i.e. at 50 minutes in Figure 6a and at 10 and 30 minutes in Figure 6b. There are significant changes in the transients at the time of these features, meaning that they are not associated with composition or structural change, but that they can be attributed to surface etching. The progressive surface etching
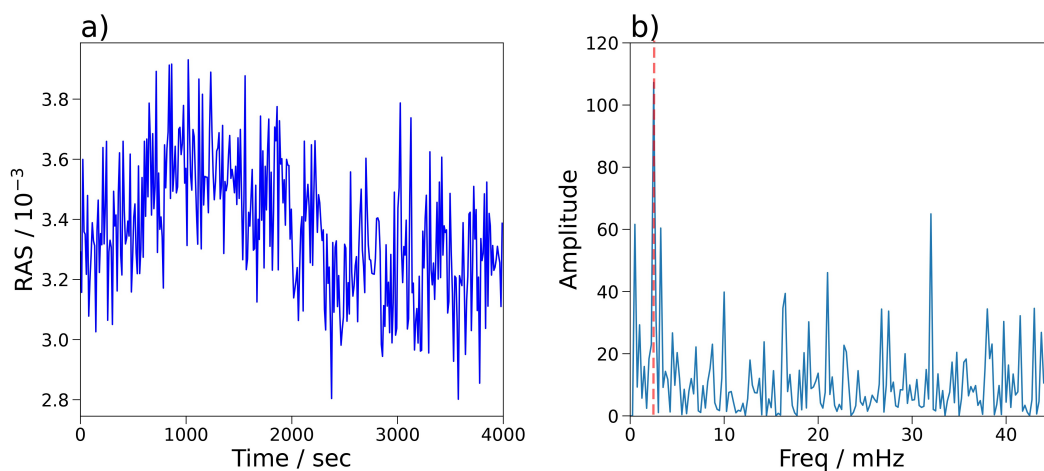
Figure 7. (a) Transient at 1.49 eV extracted from the CP from Figure 6(a) and 6(b). The corresponding Fourier spectrum. The red dashed line marks the predominant frequency of the spectrum at 2.5 mHz.

indicates that the stripping/plating is uneven. Al is more stripped than plated, and depending on the potential range used, more or less cycles are needed to fully etch one aluminum layer. Between -0.25 and 0.25 V, only one step-wise increase in the DC signal is observed, while between -0.5 and 0.5 V, 2 step-wise increases can be observed before the process becomes too ill-defined and it is not possible to distinguish features from etching anymore. Hence, the potential range and the scan rate also have an impact on the occurrence of surface etching.

While in this study both single- and poly-crystalline substrates have comparable CVs, using different crystal orientations can result in different cycling performance. This difference in structural form can impact the physical properties of the deposited Al, such as its grain size, grain boundaries, and defect density. This impacts the nucleation and growth of Al deposits, altering the overall electrochemical behaviour. Dendrite formation during Al electrodeposition depends on factors like surface properties of the aluminum substrate, electrolyte, and cycling conditions, and results from inhomogeneous current distribution, ion concentration variations, and defects.[39–41] Single crystals offer defined nucleation sites, promoting or inhibiting dendrite growth based on their surface orientation. As displayed in Figure S7, dendrites were observed on the SEM images of the crystal C2 taken after the experimental series described in Figure S1 was conducted. It means that, depending on the electrochemical conditions, an Al 110-orientation is prone to dendrite growth in a [EMImCl]:AlCl$_3$ (1:1.5) electrolyte. Structural changes from nanocrystalline to microcrystalline aluminum can influence dendrite formation as well. Microcrystalline structures reduce nucleation sites, but may have defects that promote dendrites. Al(110) sample C3 was cycled in smaller potential ranges (where plating/stripping in the nanocrystalline form of Al is predominant) and at lower scan rates than the crystal C2. Unlike for the ones of C3, the SEM images from Figure S7 of C2 present dendrites, meaning that the dendrite growth is favoured by a microcrystalline surface structure.

These findings show that RAS can be used as a probe to study electrochemical interfaces of battery systems comprising stripping/plating, SEI formation, and dendrite growth. Note that since the interfaces of battery systems remain very challenging and are still at an early stage of investigation and comprehension, interpretation and conclusion from RAS investigation should be accompanied by complementary techniques such as XPS, STM, and 2D-SOR. Nevertheless, this study gives a glimpse into the potential of electrochemical RAS as a complementary tool for the study of battery-electrolyte interfaces and interphases. Specifically, it enlightens the etching process and morphological changes at the Al(110)-IL interface during electrochemical conditioning.

Conclusions

In this work, we introduced RAS as an *in situ* technique of the Al(110)-electrolyte interface monitoring for battery applications.

We particularly showed that the surface pre-treatment in [EMImCl]:AlCl$_3$ affects the reflectance at the interface and the anisotropic feature of the Al(110) spectrum related to its oxide passivation layer. In the electrolyte, although the Al surface globally deteriorates due to electrolyte decomposition and swelling of the passivation layer, a localized surface ordering progressively rises over the pre-treatment. Comparison of the surface before and after pre-treatment with the computed spectra and with post-mortem SEM/EDX analysis allows deducing a combination of a partial decrease in the passivation layer thickness and the appearance of active sites with an overall increase in surface roughness/inhomogeneities. Al stripping/plating from the [EMImCl]:AlCl$_3$ electrolyte on Al(110) single crystals is comparable to polycrystalline Al foil and evolves from nanocrystalline to a microcrystalline form of Al. The CVs of the pre-treated Al(110) electrode exhibit a faster stabilization of Al plating and stripping peaks compared to those of untreated Al(110). This observation suggests that for an Al crystal with a 110-orientation, the pre-treatment has a positive effect on the Al plating and stripping performances.

The presence of oscillations of the anisotropy during plating and stripping was only observed in a low potential range. It suggests that, depending on the potential range, the stripping and plating process is more or less ordered. Cycling in a potential range, where Al plating and stripping in the nano-crystalline form is predominant, occurs in a more defined manner than cycling in a potential range where Al plating and stripping in the microcrystalline form is preponderant.

Yet the Al-[EMImCl]:AlCl$_3$ interface remains very complex, and the use of [EMImCl]:AlCl$_3$ for a high AlCl$_3$/[EMImCl] ratio is highly corrosive and therefore not sustainable for long-term battery operation. This study emphasizes that RAS is a potential tool to follow the build-up of a conductive and protective film which is required for the implementation of non-acidic, non-aqueous electrolytes.[9] A natural progression of this work is to improve the pre-treatment of noisy signals. As an alternative, focusing on advanced light sources could increase signal-to-noise ratios.

Experimental

Materials and electrolyte preparation

The Al(110) single crystals were purchased from Mateck (purity of 99,999%, diameter of 10 mm, and thickness of 3 mm) and are denoted as C1, C2 and C3. In the study, [EMImCl]:AlCl$_3$ (1:1.5) was prepared by slowly adding aluminum chloride (AlCl$_3$) (Anhydrous, Sigma–Aldrich, 99.99%) to 1-Ethyl-3-methylimidazolium chloride (EMImCl) (Sigma–Aldrich, >95%) while stirring using a magnetic stirring bar at room temperature (28 to 30°C) inside an argon-filled glovebox (MBraun, <0.5 ppm O$_2$, <0.5 ppm H$_2$O). Anhydrous Acetonitrile (99.8%) has been purchased from Sigma–Aldrich.

Al surface pre-treatment

All handling and preparation of Al(110) occurred inside an argon-filled glovebox. The Al electrode surface modification has been achieved by immersion for 2 hours in 6 mL of [EMImCl]:AlCl$_3$ (1:1.5)

Batteries & Supercaps

Research Article
doi.org/10.1002/batt.202300394

Chemistry Europe
European Chemical
Societies Publishing

electrolyte. Spectra were taken prior to, during and after surface pre-treatment, in the absence and presence of electrolyte. After each measurement, the Al(110) was cleaned and washed several times with anhydrous acetonitrile inside the glovebox before the RA spectrum was measured.

Electrochemical setup and technique

All electrochemical experiments were performed inside an argon-filled glovebox. For the electrochemical measurement, a photo-electrochemical cell (PEC cell) from Zahner was used for C2 and a Raman cell from rhd instruments was used for C3. For the PEC cell, Al wire as a pseudo reference electrode Alfa Aesar (0.5 mm diameter, 99.9999% purity) and glassy carbon as counter electrode (redox.me) were respectively polished with SiC paper (400 P WS FLEX 16) and 250 nm diamond polishing suspension (rhd instruments) before each electrochemical setup. The PEC and the rhd cell were filled with 9 and 3 ml of [EMImCl]:AlCl$_3$ (1:1.5), respectively. For the RA spectroscopy, an EpiRAS from Laytec was employed. The electrochemical measurements were controlled with a Princeton Applied Research VersaSTAT 3F potentiostat and a Gamry Instruments (Interface 5000E). To perform the measurements, the RA-spectrometer was installed on top of the glovebox. A quartz window placed in the sealing of the glovebox, between the setup and the spectrometer, allowed light transmission. The electrochemical cell was placed under the window on top of a hexapod (Physik Instrumente H-840 Hexapod), which allowed for rotating, inclining, and translating the cell to align it with the lightpath. For the SEM/EDX measurements the Apero 2 from Thermo Fisher Scientific with the clean connect system was used, enabling transport of the sample from the glovebox to the SEM without breaking the inert environment. The SEM/EDX measurements were done with a 10 kV electron beam and a beam current of 26 nA. The experimental series performed with C2 are detailed in Figure S1.

Baseline correction and FFT

A baseline correction was applied to some spectra, using a Si(100) crystal immersed in the electrolyte. The transients from Figure 7 are filtered by Fast Fourier transform (FFT) with an exponential filter of a factor of −0.5.

Computational

To obtain theoretically derived RAS, we firstly performed density-functional theory (DFT) calculations with Quantum Espresso (QE).[42] In the QE, we adopted the optimized norm-conserving Vanderbilt pseudopotentials. The sampling of the Brillouin zone (BZ) was performed with a 40×120×1 **k**-grid for our investigated systems. An energy cutoff of 50 Ry was used. For the exchange-correlation functional, we employed the generalized gradient approximation (GGA) in the Perdew–Burke–Ernzerhof (PBE) parametrization. The subsequent RAS calculations were carried out using the Yambo code.[43,44] Here, we used the IP-RPA method to compute the dielectric function of our investigated slabs.

Supporting Information

The authors have cited additional references within the Supporting Information.[10,46]

Conflict of Interests

There are no conflicts to declare.

Data Availability Statement

The data that support the findings of this study are openly available on Zenodo at https://doi.org/10.5281/zenodo.10000855, Ref. [45].

[1] B. Craig, T. Schoetz, A. Cruden, C. Ponce de Leon, *Renewable Sustainable Energy Rev.* **2020**, *133*, 110100.
[2] Q. Li, N. J. Bjerrum, *J. Power Sources* **2002**, *110*, 1.
[3] E.-S. Lee, S.-H. Huh, S.-H. Lee, S.-H. Yu, *ACS Sustainable Chem. Eng.* **2023**, *11*, 2014.
[4] X. Zhang, R. Lv, W. Tang, G. Li, A. Wang, A. Dong, X. Liu, J. Luo, *Adv. Funct. Mater.* **2020**, *30*, 2004187.
[5] S. K. Das, S. Mahapatra, H. Lahan, *J. Mater. Chem. A* **2017**, *5*, 6347.
[6] C. Schütter, A. Bothe, A. Balducci, *Electrochim. Acta* **2020**, *331*, 135421.
[7] M. Chiku, S. Matsumura, H. Takeda, E. Higuchi, H. Inoue, *J. Electrochem. Soc.* **2017**, *164*, A1841.
[8] J.-K. Chang, S.-Y. Chen, W.-T. Tsai, M.-J. Deng, I.-W. Sun, *Electrochem. Commun.* **2007**, *9*, 1602.
[9] L. C. Loaiza, N. Lindahl, P. Johansson, *J. Electrochem. Soc.* **2023**, *170*, 030512.
[10] T. Mandai, P. Johansson, *J. Mater. Chem. A* **2015**, *3*, 12230.
[11] Z. Slim, E. J. Menke, *Batteries & Supercaps* **2023**, *6*, e202300164.
[12] X. Wen, J. Zhang, H. Luo, J. Shi, C. Tsay, H. Jiang, Y.-H. Lin, M. A. Schroeder, K. Xu, J. Guo, *J. Phys. Chem. Lett.* **2021**, *12*, 5903.
[13] H. Wang, S. Gu, Y. Bai, S. Chen, F. Wu, C. Wu, *ACS Appl. Mater. Interfaces* **2016**, *8*, 27444.
[14] S. Varshney, M. Oded, S. Remennik, V. Gutkin, U. Banin, *Small* **2023**, *19*, 2304478.
[15] R. Tao, H. Fu, C. Gao, L. Fan, E. Xie, W. Lyu, J. Zhou, B. Lu, *Adv. Funct. Mater.* **2023**, 2303072.
[16] S. He, J. Wang, X. Zhang, W. Chu, S. Zhao, D. He, M. Zhu, H. Yu, *J. Mater. Chem. A* **2023**, *11*, 17020.
[17] F. Wu, N. Zhu, Y. Bai, Y. Gao, C. Wu, *Green Energy & Environ.* **2018**, *3*, 71.
[18] H. Wang, S. Gu, Y. Bai, S. Chen, F. Wu, C. Wu, *ACS Appl. Mater. Interfaces* **2016**, *8*, 27444.
[19] T. Dong, K. L. Ng, Y. Wang, O. Voznyy, G. Azimi, *Adv. Energy Mater.* **2021**, *11*, 2100077.

Batteries & Supercaps

Research Article
doi.org/10.1002/batt.202300394

Chemistry
Europe

European Chemical
Societies Publishing

[20] K. Haberland, P. Kurpas, M. Pristovsek, J.-T. Zettler, M. Weyers, W. Richter, *Appl. Phys. A Mater. Sci. Process.* **1999**, *68*, 309.

[21] P. Weightman, D. S. Martin, R. J. Cole, T. Farrell, *Rep. Prog. Phys.* **2005**, *68*, 1251.

[22] M. Guidat, M. Löw, M. Kölbach, J. Kim, M. M. May, *ChemElectroChem* **2023**, *10*, e202300027.

[23] J. Scherer, O. Magnussen, T. Ebel, R. Behm, *Corros. Sci.* **1999**, *41*, 35.

[24] T. Herrmann, M. Gensch, M. J. G. Lee, A. I. Shkrebtii, N. Esser, W. Richter, P. Hofmann, *Phys. Rev. B* **2004**, *69*, 165406.

[25] C. Hogan, O. Pulci, P. Gori, F. Bechstedt, D. S. Martin, E. E. Barritt, A. Curcella, G. Prevot, Y. Borensztein, *Phys. Rev. B* **2018**, *97*, 195407.

[26] S. Poetz, P. Handel, G. Fauler, B. Fuchsbichler, M. Schmuck, S. Koller, *RSC Adv.* **2014**, *4*, 6685.

[27] D.-M. She, W.-L. Song, J. He, N. Li, H. Chen, S. Jiao, D. Fang, *J. Electrochem. Soc.* **2020**, *167*, 130530.

[28] P. M. Natishan, W. E. O'Grady, *J. Electrochem. Soc.* **2014**, *161*, C421.

[29] *Buehler Sum Met: The Sum Of Our Experience*, Buehler, Lake Bluff, Il, 4th edition **2018**.

[30] C. Punckt, F. S. Merkt, H. H. Rotermund, *New J. Phys.* **2007**, *9*, 213.

[31] S. Pfaff, A. Larsson, D. Orlov, G. S. Harlow, G. Abbondanza, W. Linpé, L. Rämisch, S. M. Gericke, J. Zetter-berg, E. Lundgren, *ACS Appl. Mater. Interfaces* **2021**, *13*, 19530.

[32] R. Böttcher, S. Mai, A. Ispas, A. Bund, *J. Electrochem. Soc.* **2020**, *167*, 102516.

[33] D. Pradhan, D. Mantha, R. Reddy, *Electrochim. Acta* **2009**, *54*, 6661.

[34] H. Yang, F. Wu, Y. Bai, C. Wu, *J. Energy Chem.* **2020**, *45*, 98.

[35] S. Xia, X. Zhang, K. Huang, Y.-L. Chen, Y. Wu, *J. Electroanal. Chem.* **2015**, *757*.

[36] O. M. Ylivaara, X. Liu, L. Kilpi, J. Lyytinen, D. Schneider, M. Laitinen, J. Julin, S. Ali, S. Sintonen, M. Berdova, E. Haimi, T. Sajavaara, H. Ronkainen, H. Lipsanen, J. Koskinen, S.-P. Hannula, R. L. Puurunen, *Thin Solid Films* **2014**, *552*, 124.

[37] M. Jiang, C. Fu, P. Meng, J. Ren, J. Wang, J. Bu, A. Dong, J. Zhang, W. Xiao, B. Sun, *J. Adv. Mater.* **2022**, *34*, 2102026.

[38] M. Löw, M. Guidat, J. Kim, M. M. May, *RSC Adv.* **2022**, *12*, 32756.

[39] N. Sabi, K. Palanisamy, F. Rahide, S. Daboss, C. Kranz, S. Dsoke, *Batteries & Supercaps* **2023**, *6*, e202300298.

[40] N. Li, D. She, K. Zhang, H.-S. Chen, W.-L. Song, S. Jiao, *ChemSusChem* **2022**, *15*, e202201390.

[41] T. Schoetz, O. Leung, C. P. De Leon, C. Zaleski, I. Efimov, *J. Electrochem. Soc.* **2020**, *167*, 040516.

[42] P. Giannozzi, S. Baroni, N. Bonini, M. Calandra, R. Car, C. Cavazzoni, D. Ceresoli, G. L. Chiarotti, M. Cococcioni, I. Dabo, A. D. Corso, S. de Gironcoli, S. Fabris, G. Fratesi, R. Gebauer, U. Gerstmann, C. Gougoussis, A. Kokalj, M. Lazzeri, L. Martin-Samos, N. Marzari, F. Mauri, R. Mazzarello, S. Paolini, A. Pasquarello, L. Paulatto, C. Sbraccia, S. Scandolo, G. Sclauzero, A. P. Seitsonen, A. Smogunov, P. Umari, R. M. Wentzcovitch, *J. Phys. Condens. Matter* **2009**, *21*, 395502.

[43] A. Marini, C. Hogan, M. Grüning, D. Varsano, *Comput. Phys. Commun.* **2009**, *180*, 1392.

[44] D. Sangalli, A. Ferretti, H. Miranda, C. Attaccalite, I. Marri, E. Cannuccia, P. Melo, M. Marsili, F. Paleari, A. Marrazzo, G. Prandini, P. Bonfà, M. O. Atambo, F. Affinito, M. Palummo, A. Molina-Sánchez, C. Hogan, M. Grüning, D. Varsano, A. Marini, *J. Phys. Condens. Matter* **2019**, *31*, 325902.

[45] M. Guidat, F. Rahide, M. Loew, J. Kim, H. Ehrenberg, S. Dsoke, M. M. May, *Zenodo dataset* **2023**, DOI:10.5281/zenodo.10000854.

[46] F. Rahide, E. Zemlyanushin, G.-M. Bosch, S. Dsoke, *J. Electrochem. Soc.* **2023**, *170*, 030546.